Science Advances
AAAS

advances.sciencemag.org/cgi/content/full/5/9/eaaw0672/DC1

# Supplementary Materials for

## Albumin-chaperoned cyanine dye yields superbright NIR-II fluorophore with enhanced pharmacokinetics

Rui Tian, Qiao Zeng, Shoujun Zhu*, Joseph Lau, Swati Chandra, Robert Ertsey, Kenneth S. Hettie, Tarn Teraphongphom, Zhubin Hu, Gang Niu, Dale O. Kiesewetter, Haitao Sun*, Xiaodong Zhang, Alexander L. Antaris, Bernard R. Brooks, Xiaoyuan Chen*

*Corresponding author. Email: sjzhu@jlu.edu.cn (S.Z.); shawn.chen@nih.gov (X.C.); htsun@phy.ecnu.edu.cn (H.S.)

Published 13 September 2019, *Sci. Adv.* **5**, eaaw0672 (2019)
DOI: 10.1126/sciadv.aaw0672

**This PDF file includes:**

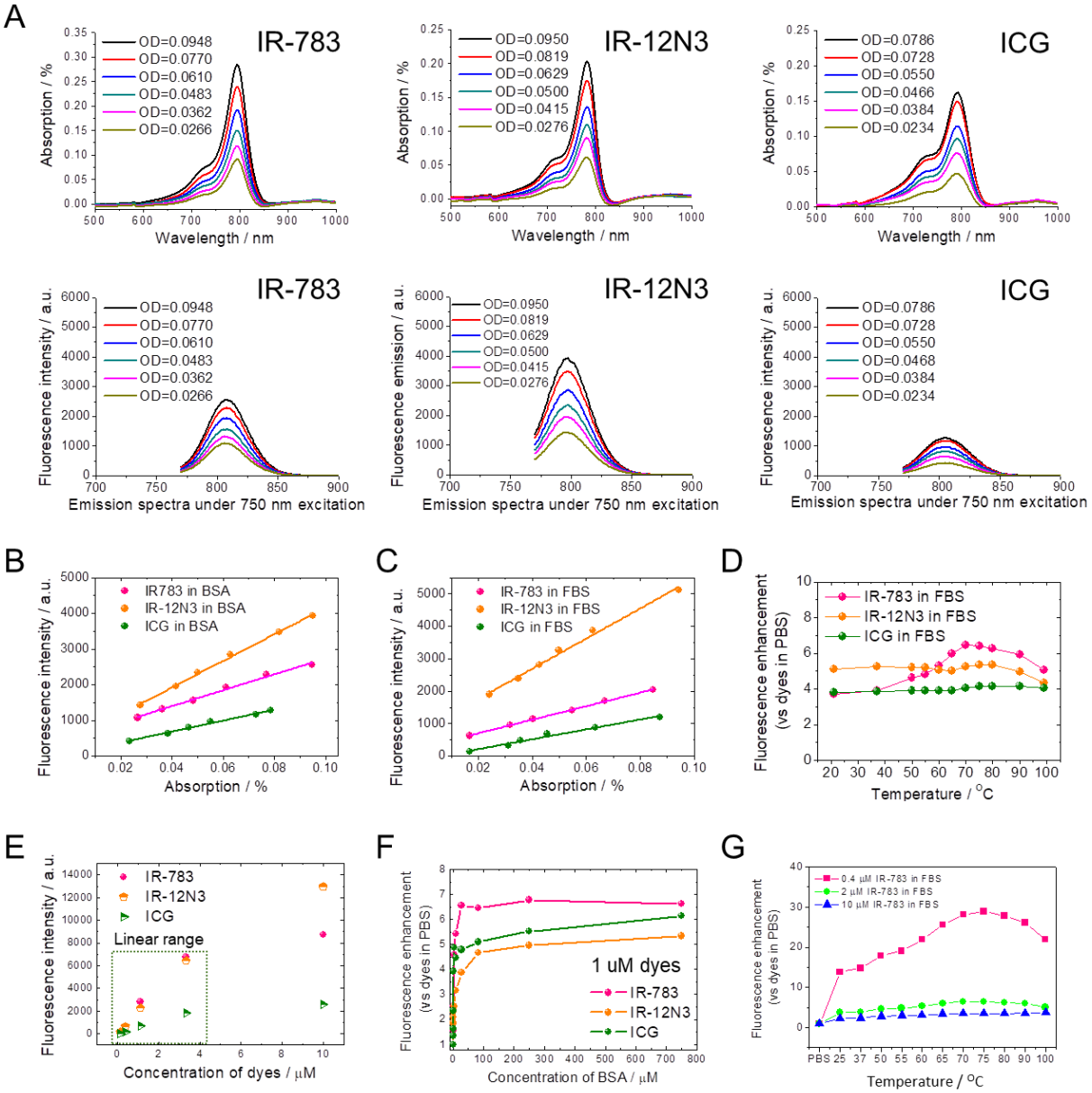


**Fig. S1. Relative QYs of IR-783, IR-12N3, and ICG in BSA/FBS, depicted by the slope of fluorescence intensity versus absorption.** (**A**) Quantum yield measurement of IR-783, IR-12N3, and ICG in 100 μM BSA (*15, 41*). (**B**) Quantum yield comparison (slope method) of IR-783, IR-12N3, and ICG in BSA (100 μM). (**C**) Quantum yield comparison of IR-783, IR-12N3, and ICG in FBS. (**D**) Brightness enhancement after heating for 10 min of dyes pre-mixed with FBS. (**E**) The relationship between the fluorescence intensity and concentration of dyes shows the linear range is below 4 μM (PBS) (*15*). (**F**) The relationship between fluorescence enhancement and BSA concentration (free mixture of 1 μM dye with BSA in PBS), and the maximum enhancement in BSA is 6-7 folds. (**G**) The fluorescence enhancement in FBS is temperature dependent, affording approximately 23-fold increase at 60 ˚C at lower concentrations of dye.

**Note:** The relative quatum yield was determined by the slope in B and C. The FBS/PBS ratio = fluorescence intensity of complex in FBS / fluorescence intensity of complex in PBS.
When dispersing the equivalent dosages at less than 0.4 μM in both PBS and FBS buffer respectively, the brightness of complex in FBS will be higher than in PBS if there is free dye escaped from the complex.

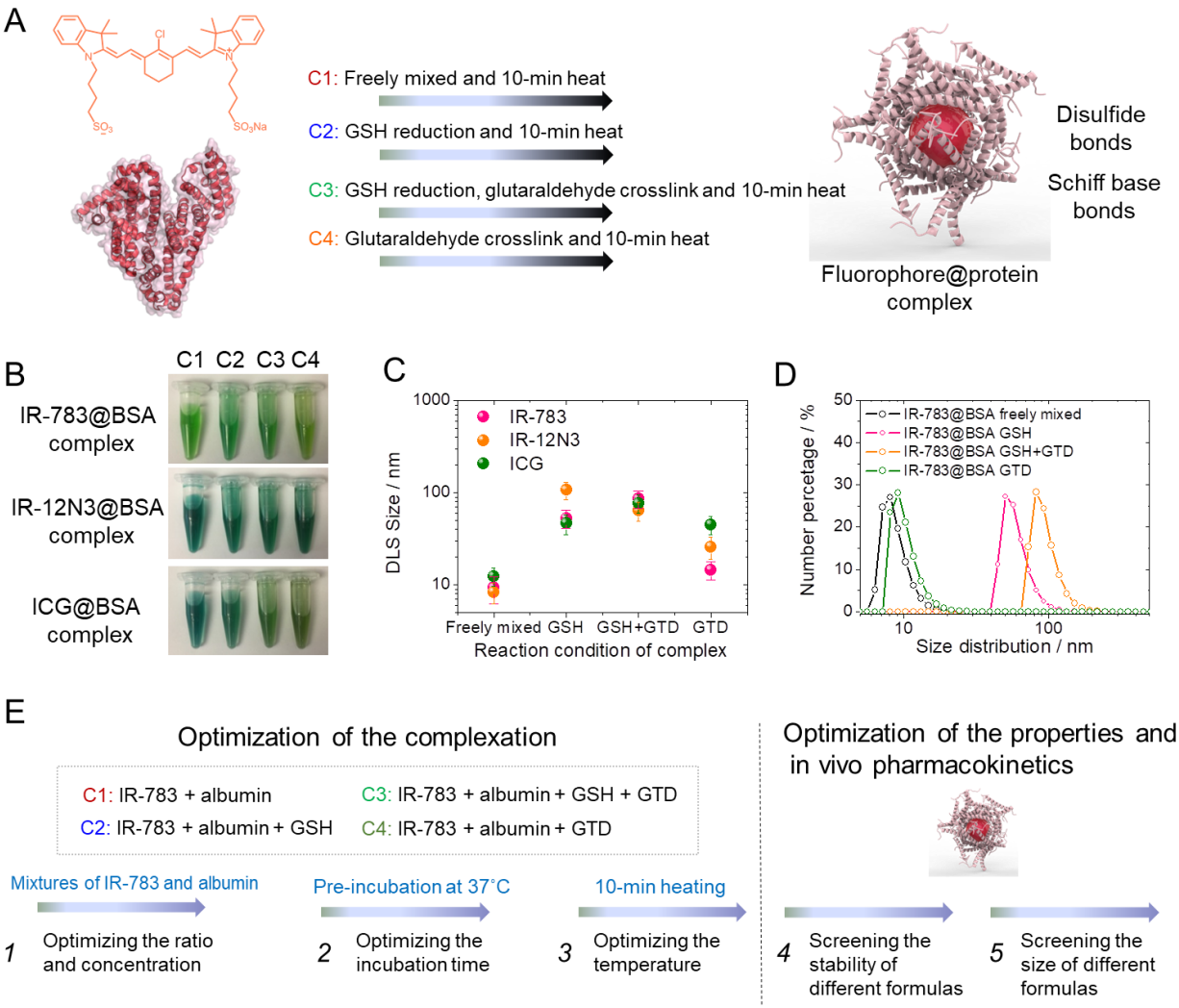


**Fig. S2. Method optimization for the fluorophore@BSA complex.** (**A**) Scheme of four reaction conditions. Four reaction conditions (freely mixed, GSH, GSH+GTD, or GTD) with 10-min heat were applied to optimize the complex of BSA with three fluorophores. (**B**) Digital pictures of fluorophore@BSA complexes. (**C**) DLS size of fluorophore@BSA complexes. IR-783@BSA complex is more stable than the other two complexes. (**D**) Typical DLS size of IR-783@BSA complexes at four reaction conditions, respectively. (**E**) Scheme of the procedure for optimizing the complexation.

**Note:**

1. Although not achieved in the current work, the BSA can also be replaced by HSA with the similar protein structure.
2. There are several key literatures in terms of cyanine dye binding to albumin which invariably focus on traditional NIR-I imaging window (*30, 31, 42-47*). We can also adopt the successful experience on albumin-drug system (*29, 32, 33, 48-50*). The key novelty of the present work focuses on developing new NIR-II contrast agent through several improved albumin-binding strategies, and it is very important to screen an optimal strategy to synthesize the bright NIR-II albumin-complex agent.

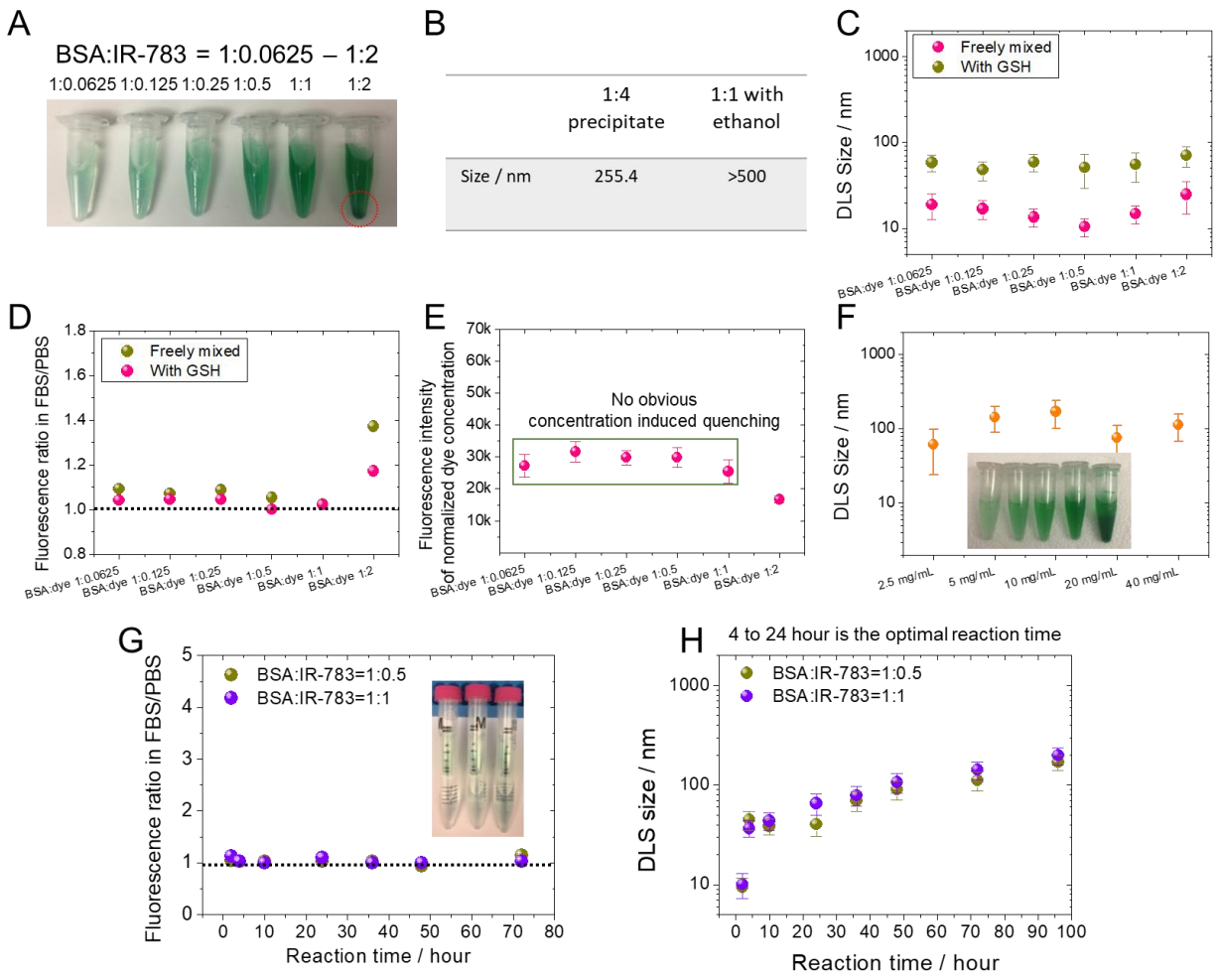


**Fig. S3. The optimization for ratio and reaction concentration of BSA and IR-783.** (**A**) The BSA to IR-783 ratio was tuned from 1:0.0625, 1:0.125, 1:0.25, 1:0.5, 1:1 to 1:2 and the pictures of the final complexes were listed. Some aggregation appeared in the complex of 1:2 ratio. (**B**) For 1:4 ratio and 1:1 ratio with adding ethanol (typical treatment in the literature), the size of the final complex is over 200 nm. (**C**) The DLS size of the complex (condition 2 with GSH) was optimized below 100 nm for ratios of BSA: dye below 1:2. (**D**) The stability of the complex was optimized below the BSA: dye ratio of 1:2. (**E**) The fluorescence intensity remained constant until reaching higher ratio close to 1:2. (**F**) The reaction concentration was controlled under 20 mg/ml of BSA due to the obvious aggregation/crosslink when using 40 mg/ml. (**G**) The fluorophore@BSA complex remained stable from 4 hours to approximately 70 hours of reaction time. (**H**) The size of the complex was optimized to between 30 to 100 nm at a reaction time of 4 to 36 hours. Short time reaction cannot afford enough reaction capacity with less stable feature while long reaction time caused crosslink to large nano-complex over 100 nm.

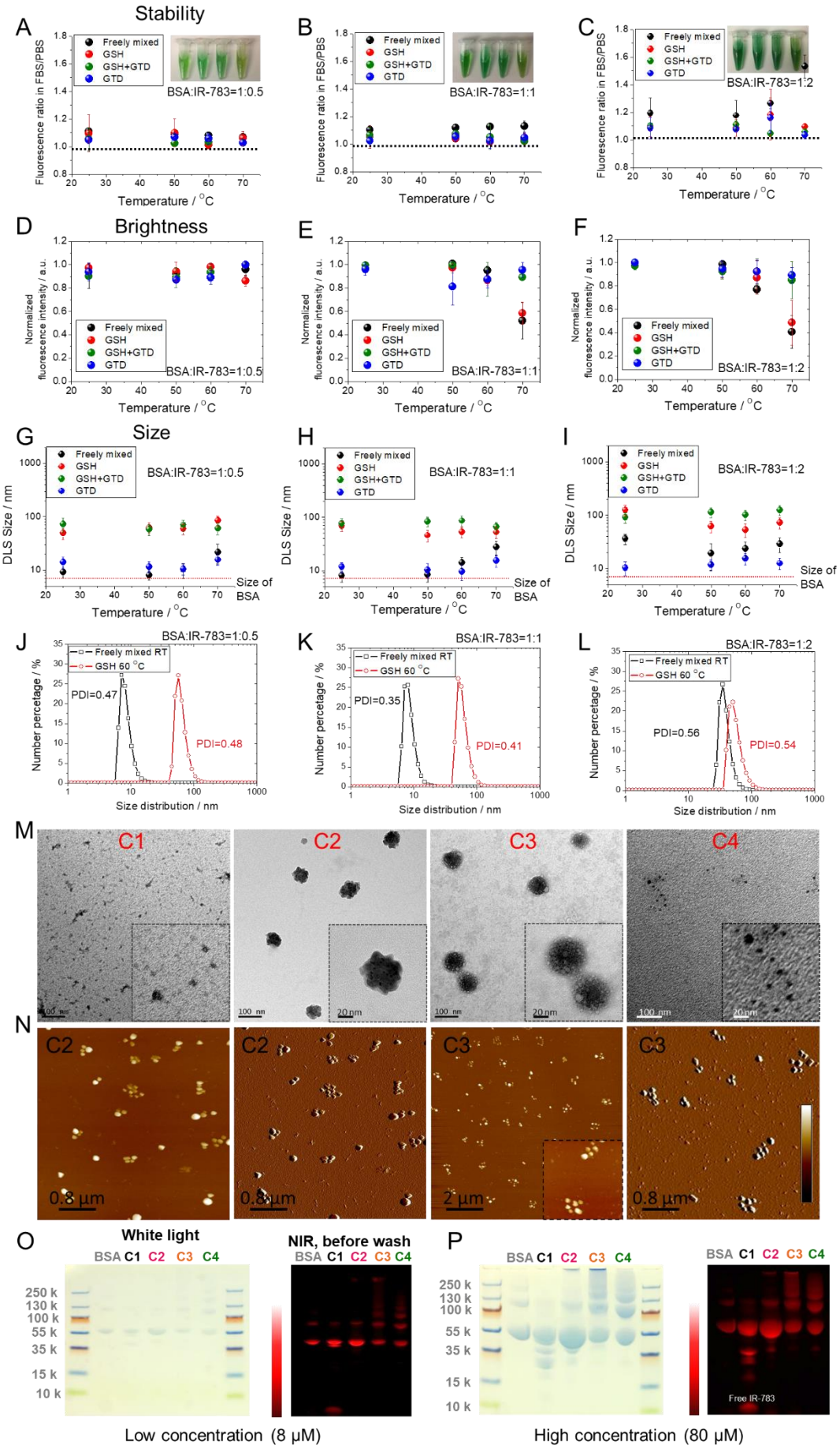
A
Stability
Freely mixed
GSH
GSH+GTD
GTD
BSA:IR-783=1:0.5
Fluorescence ratio in FBS/PBS
Temperature / °C
B
BSA:IR-783=1:1
C
BSA:IR-783=1:2
D
Brightness
Normalized fluorescence intensity / a.u.
E
F
G
Size
DLS Size / nm
Size of BSA
H
I
J
BSA:IR-783=1:0.5
Freely mixed RT
GSH 60 °C
PDI=0.47
PDI=0.48
Number percetage / %
Size distribution / nm
K
BSA:IR-783=1:1
PDI=0.35
PDI=0.41
L
BSA:IR-783=1:2
PDI=0.56
PDI=0.54
M
C1
C2
C3
C4
100 nm
20 nm
N
0.8 μm
2 μm
O
White light
NIR, before wash
BSA C1 C2 C3 C4
250 k
130 k
100 k
55 k
35 k
15 k
10 k
Low concentration (8 μM)
P
Free IR-783
High concentration (80 μM)

**Fig. S4. Stability, brightness, and size of the IR-783@BSA complex at 1:0.5, 1:1, and 1:2 ratios.** Fluorophore@BSA complex was more stable (fluorescence ratio in FBS/PBS is close to 1) at (**A**) 1:0.5 and (**B**) 1:1 ratios of BSA:IR-783 than the (**C**) 1:2 ratio. Reaction condition C2-C4 (GSH, GSH+GTD, GTD) produced much stable complexes compared with C1 (freely mixed). The complex showed more decent brightness at (**D**) 1:0.5, (**E**) 1:1, and (**F**) 1;2 ratios of BSA:IR-783 below 70 $^{O}$C. The DLS analysis showed the size of IR-783@BSA complex at (**G** and **J**) 1:0.5, (**H** and **K**) 1:1 and (**I** and **L**) 1:2 ratios. C2 and C3 (GSH, GSH+GTD) afforded complexes with sub-100 nm size compared with C1 and C4 with 10-20 nm size distribution. Fluorophore: BSA complex is below 100 nm at (a) 1:0.5 and (b) 1:1 ratios of BSA: IR-783, but not as consistently for the (c) 1:2 ratio. (**M**) Transmission electron microscopy (TEM) analysis of formation of the four different formulations of fluorophore@BSA complexes. (**N**) Atomic force microscopy (AFM) analysis of formation of the different formulations of fluorophore@BSA complexes. (**O-P**) Electrophoresis gel analysis of IR-783@BSA complexes (BSA: IR-783= 1:1) at the concentration of 8 μM in (**O**) and 80 μM in (**P**). Electrophoresis testing indicated that monomer, dimer, trimer and large-size nano-complex existed. The very top bands are the large-size nanoparticles observed in DLS testing.

**Note:**

1. The heating temperature was optimized to 60 $^{O}$C according to both the stability and brightness performance (also see electrophoresis result in Fig. 1G in main text). High post-heated temperature (>70 $^{O}$C) suffered from decrease of the brightness.
2. The true size distribution of final complex included monomer, dimer, trimer and nano-complex. We conducted density gradient centrifugation (DGU) to purify the monomer and large size nano-complex. As a result, the DLS only observed the population of large size.
3. For DGU, the final complex was subjected to DGU purification. Sucrose column gradient for 4 mL DGU tube was made by interval adding: 10, 15, 20, 25, 30, 35, 40 % (400 μL of each and then tilt-permeate), then subject to ultracentrifuge for 18 hours at 50000 rpm and 4 ℃. Sucrose column gradient for 50 mL DGU tube was made by gradient maker: from 20% to 50 % (16 mL). 5 mL 60 % sucrose was firstly added at the bottom of the tube before forming gradient. Then subject to ultracentrifuge for 48 hours at 31000 rpm and 4 $^{O}$C.
4. We have confirmed that the in vivo behaviors of different size distributions were similar for each individual reaction condition. As a result, the purification is not necessary for in vivo imaging, and we can use either purified components or the raw product for further in vivo study.
5. For electrophoresis gel analysis:

(1). In the dilute samples, the top bands of large size are too weak to visualize.

(2). The reaction temperature controlled the population of large size complex. The higher post-treatment temperature applied, the more large-size complex (Fig. 1G) produced.

(3). Low reaction temperature (RT and 50 $^{O}$C) suffered from the stability issue (see free dye bands of complexes prepared from RT and 50 $^{O}$C at lower position in NIR imaging of Fig. 1G in main text).

(4). Overall, the optimal reaction condition was listed here: BSA: IR-783 = 1:0.5 or 1:1 with condition 2-4; concentration of BSA is 20 mg/ml; reaction time is 24 hours; temperature of post-treatment is 60 $^{O}$C.

6. There are two literatures (*13, 20*) reporting on albumin (FBS)/D-A-D fluorophore. However, the freely mixed method is not the optimal strategy to achieve the high-performance complex fluorophore. In addition, the D-A-D dyes have disadvantages of complicated synthesis steps and unclear biosafety concerns.

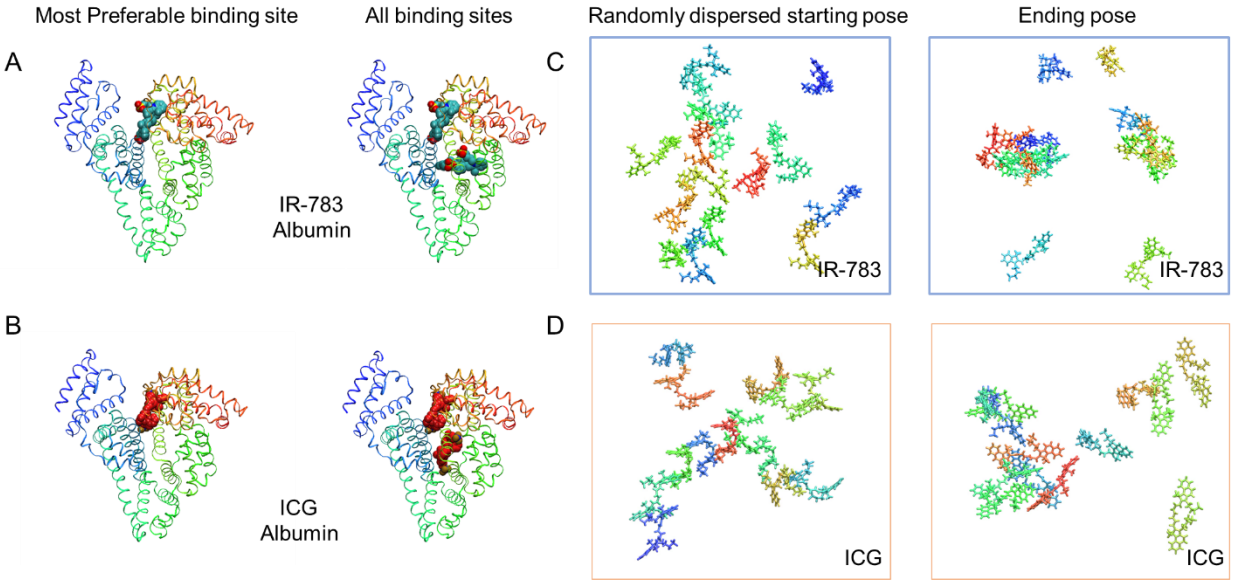


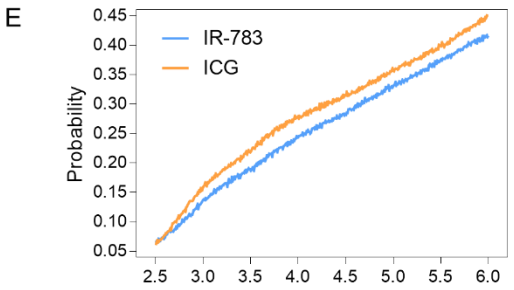


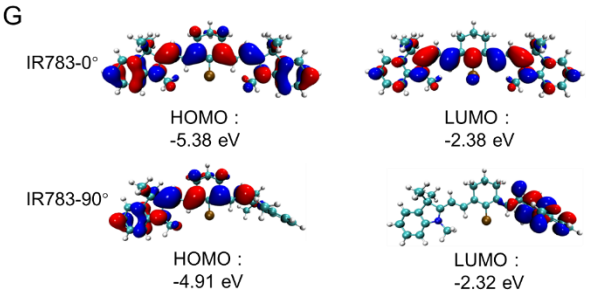


F

| mode | Affinity (kcal/mol) | Distance from best mode rmsd l.b. | rmsd u.b. |
|---|---|---|---|
| 1 | -9.2 | 0.000 | 0.000 |
| 2 | -8.8 | 18.273 | 21.876 |
| 3 | -8.7 | 14.255 | 15.759 |
| 4 | -8.6 | 12.028 | 13.709 |
| 5 | -8.6 | 18.308 | 20.582 |
| 6 | -8.0 | 1.766 | 2.096 |
| 7 | -7.9 | 13.625 | 15.094 |
| 8 | -7.8 | 13.922 | 15.434 |
| 9 | -7.6 | 18.071 | 21.685 |

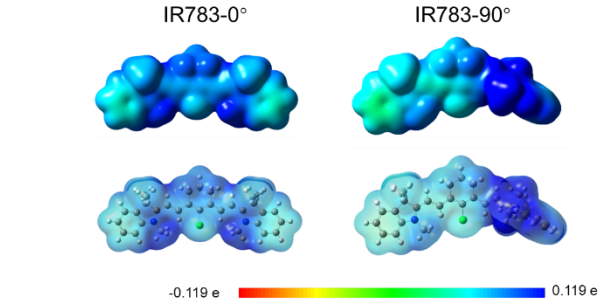


I

| Emission | Wavelength (nm) | Exp (nm) | Electronic configuration | Dihedral Angle (°) |
|---|---|---|---|---|
| NIR-I | 775 | 800 | HOMO→LUMO 100% | 6.5 |
| NIR-II | 1433 | 1100 ~1500 | HOMO→LUMO 97% | 90 |

**Fig. S5. Docking simulation and computational modeling demonstrating the binding poses and the mechanism of increased QY for complexation.** The docking model for (**A**) IR-783 and (**B**) ICG albumin with albumin, respectively. IR-783 and ICG show similar biding sites with albumin. The preferable binding site is the cleft of albumin and the secondary binding site is the site I. After randomly dispersing in the simulated water, (**C**) IR-783 showed less tendency to be self-assembling than that of (**D**) ICG using both parallel (Fig. 2C-D in main text) or random starting poses. (**E**) Radial distribution function (RDF) of ICG and IR-783, depicting that ICG had a higher tendency of self-assembly. (**F**) The simulated docking showed the distances deviation

from the best mode of different binding poses of IR-783 and partly denatured albumin. The At the docking stage, the protein was centered at the origin, and a 30 Å x 30 Å x 30 Å searching space is set for the best performance. The 3rd and 4th columns are the distance deviation from the best mode, l.b.: lower bound; u.b.: upper bound. (**G**) The HOMOs and LUMOs and (**H**) the ESP maps of IR-783 in albumin are plotted using the color range from red (−0.119 electron, negative) to blue (0.119 electron, positive). (**I**) Calculated fluorescence emission wavelength (nm) and excited-state electronic structures of IR-783 and twisted IR-783 based on time-dependent density functional theory.

**Table S1. The excitation energies for both vertical excitation and emission computed using TDDFT/IEFPCM in complex mode.** The results from both linear-response and state-specific schemes are shown to emphasize the charge-transfer effect. The corresponding states, the corresponding molecular orbital transitions, the excitation energies (ΔE), the corresponding wavelength, and the oscillator strengths for vertical excitation are listed.

| IR-783 // Trp214 | | | | | |
|---|---|---|---|---|---|
| Vertical excitation energy | | | Emission energy | | |
| Linear-response | State | S2 | Linear-response | State | S1 |
| | MO | HOMO-1→LUMO | | MO | LUMO→HOMO |
| | ΔE | 1.5093 eV | | ΔE | 1.4425 eV |
| | wavelength | 821.45 nm | | wavelength | 859.50 nm |
| | oscillator strength | 0.0107 | | | |
| State-specific | State | S2 | State-specific | State | S1 |
| | MO | HOMO-1→LUMO | | MO | LUMO→HOMO |
| | ΔE | 1.4848 eV | | ΔE | 0.8879 eV |
| | wavelength | 835.02 nm | | wavelength | 1396.32 nm |
| | Oscillator strength | 0.0105 | | | |

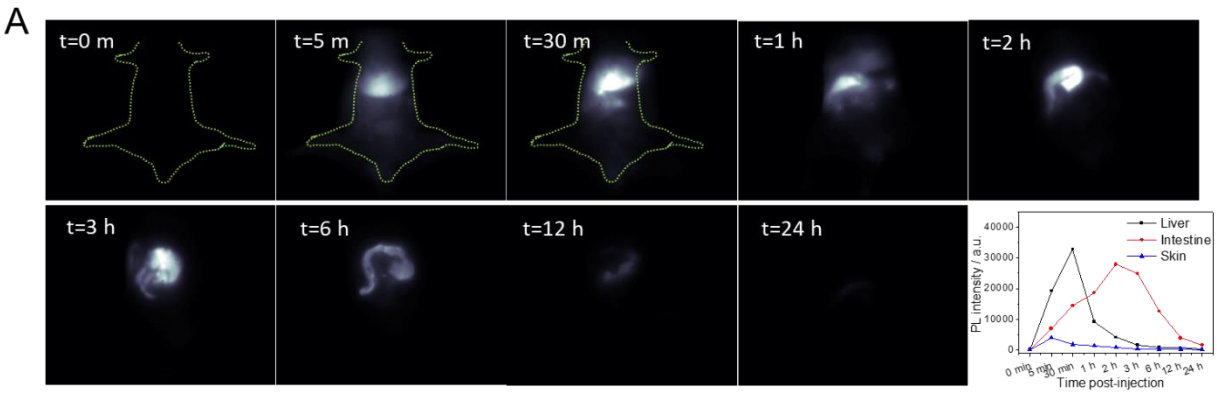
A
t=0 m
t=5 m
t=30 m
t=1 h
t=2 h
t=3 h
t=6 h
t=12 h
t=24 h
Liver
Intestine
Skin
PL intensity / a.u.
Time post-injection
0 min
5 min
30 min
1 h
2 h
3 h
6 h
12 h
24 h

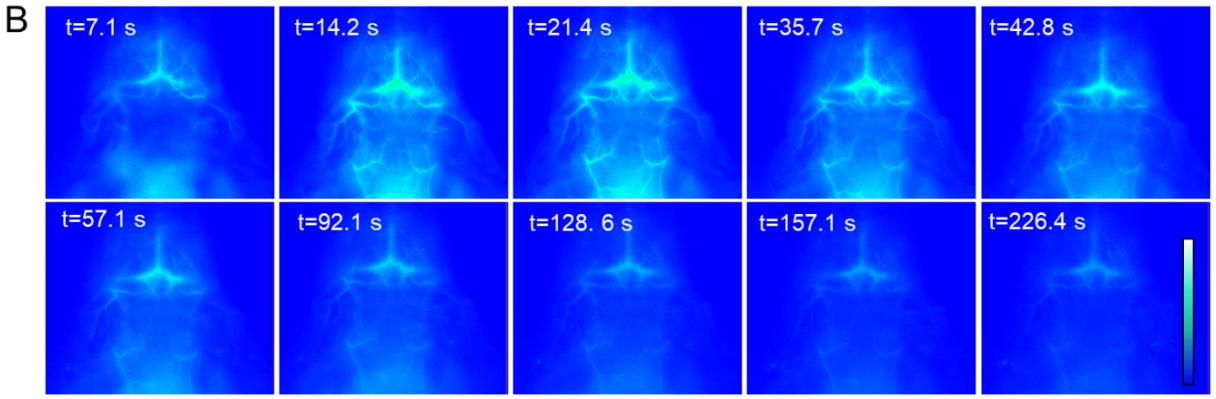
B
t=7.1 s
t=14.2 s
t=21.4 s
t=35.7 s
t=42.8 s
t=57.1 s
t=92.1 s
t=128. 6 s
t=157.1 s
t=226.4 s

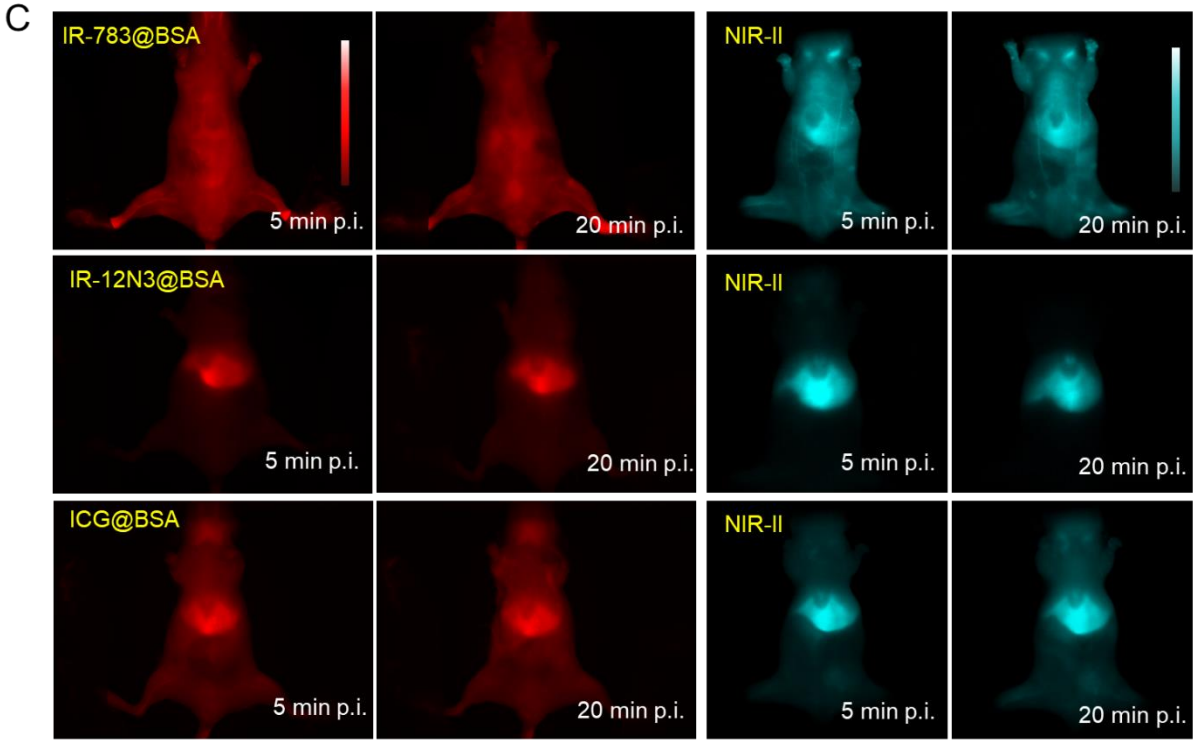
C
IR-783@BSA
5 min p.i.
20 min p.i.
NIR-II
5 min p.i.
20 min p.i.
IR-12N3@BSA
5 min p.i.
20 min p.i.
NIR-II
5 min p.i.
20 min p.i.
ICG@BSA
5 min p.i.
20 min p.i.
NIR-II
5 min p.i.
20 min p.i.

**Fig. S6. The free IR-12N3/ICG/IR-783 has quick hepatobiliary clearance and short imaging window compared to their complex with albumin.** (**A**) Typical NIR-II imaging of free IR-783 injected mouse at belly angle. Due to the fast clearance of free IR-783, the vessel imaging window is very short (less than 2 min). (**B**) Typical NIR-II brain vessel imaging of free IR-783 injection mouse with shaved head position (2.5X magnification). The signal started to diffuse and/or quench at 1.5 minutes time point post-injection. The total vessel imaging window is less than 2 min. (**C**) NIR-I (red) and NIR-II (cyan) imaging with three complexes through C2 procedure (IR-783@BSA, IR-12N3@BSA, and ICG@BSA) indicated that the IR-783@BSA showed the best vessel imaging capacity compared with the other two complexes.

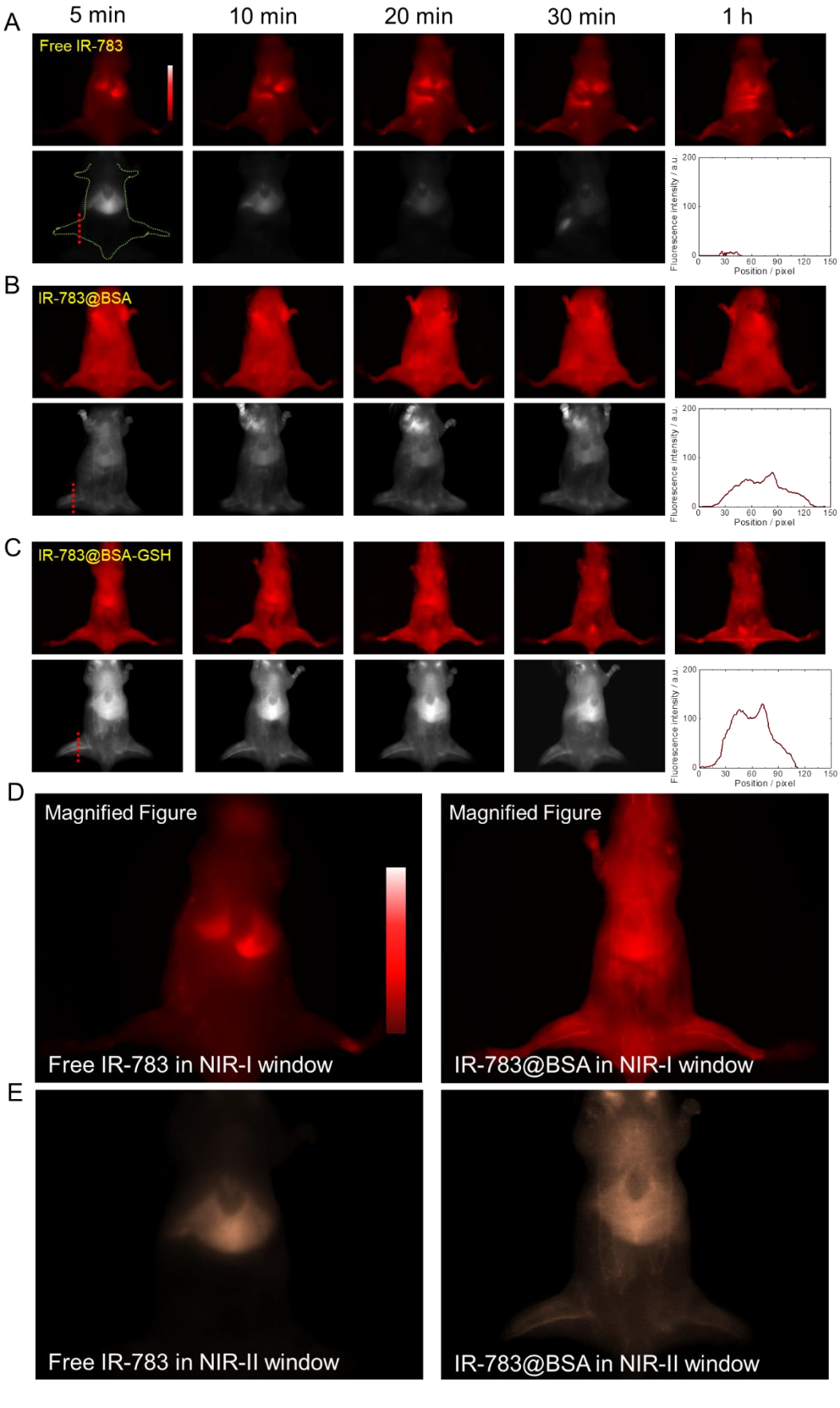
A
5 min
10 min
20 min
30 min
1 h
Free IR-783
Fluorescence intensity / a.u.
Position / pixel
B
IR-783@BSA
C
IR-783@BSA-GSH
D
Magnified Figure
Free IR-783 in NIR-I window
Magnified Figure
IR-783@BSA in NIR-I window
E
Free IR-783 in NIR-II window
IR-783@BSA in NIR-II window

**Fig. S7. Comparison of the vessel imaging time window of free IR-783 with the IR-783@BSA complex.** Whole body imaging with free (**A**) IR-783, (**B**) IR-783@BSA (C1, free mixed) and (**C**) IR-783@BSA-GSH (C2) in both NIR-I (red) and NIR-II window (grey) at increasing time point p.i.. Cross-sectional intensity profile (the dotted line) of hindlimb showed in the last panel in each group. Free IR-783 showed very quick hepatobiliary clearance while IR-783@BSA (C1, free mixed) suffered from high skin uptake with lower brightness compare with IR-783@BSA-GSG (C2). Imaging with the IR-783@BSA-GSH complex allows for an improved imaging time window (up to 1 hour) in both the NIR-I and NIR-II imaging windows and clear delineation of vessel features. High magnification images of free IR-783, IR-783@BSA-GSH in the NIR-I imaging window (**D**), and these two fluorophores in NIR-II imaging window (**E**) at 5 min p.i. time point. Sharp vessel feature was showing up in the IR-783@BSA-GSH injected mice.

**Note:** NIR-I imaging details: Complex: BSA: IR-783=1:1 with GSH; Maestro NIR I channel; 100 ms exposure time; Injection dose: 300 μM, 300 μL.
Different cohorts of mice were used for NIR-I and NIR-II imaging, respectively.

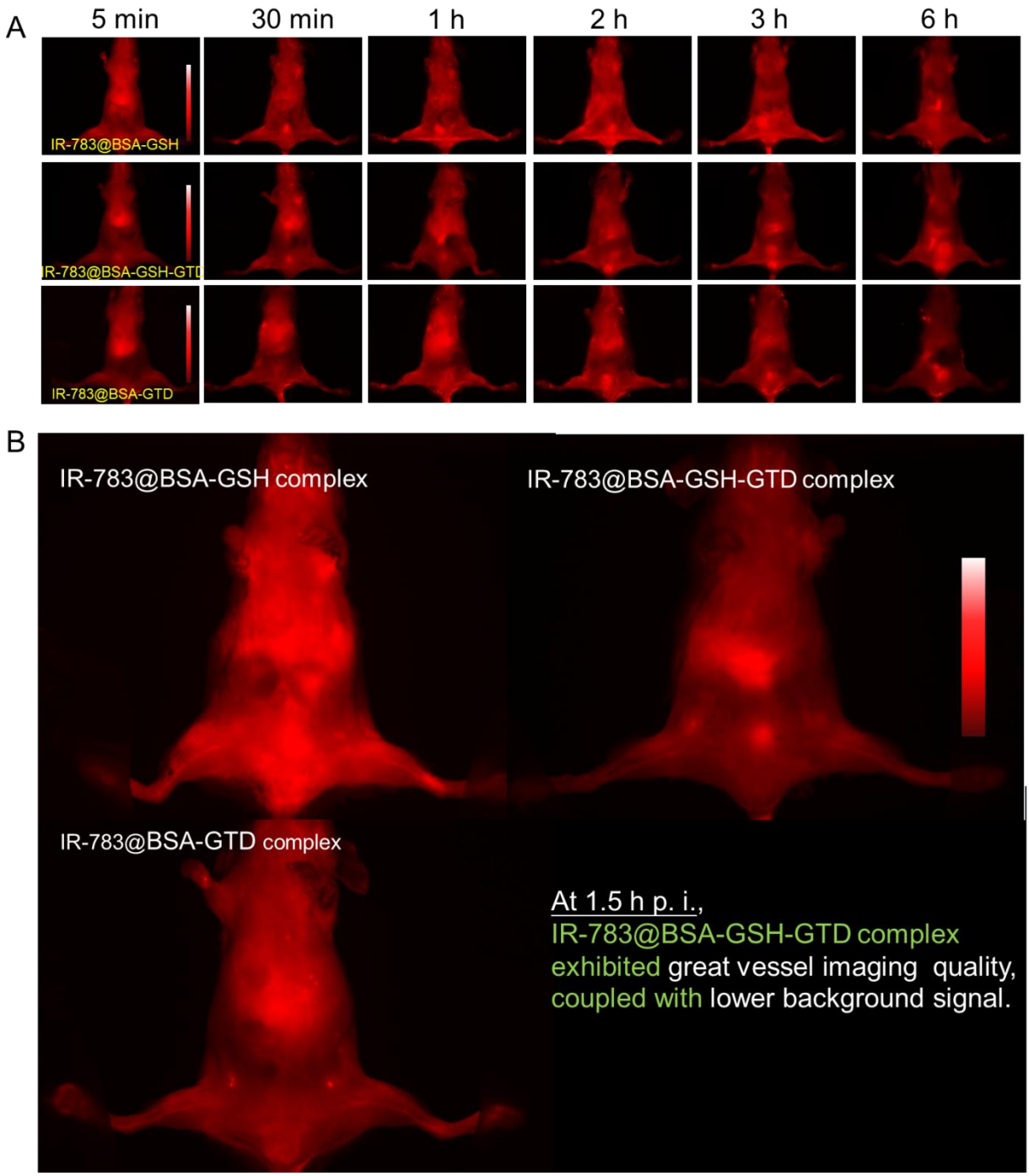


**Fig. S8. Further imaging comparison of IR-783@BSA from different conditions (C2, C3, and C4).** (**A-B**) IR-783@BSA-GSH/GTD complex can further improve the vessel imaging window up to 3 hours. Compared with IR-783@BSA-GSH and IR-783@BSA-GTD complexes, IR-783@BSA-GSH-GTD complex exhibited great vessel imaging quality, coupled with lower background signal.

**Note:** We observed there were individual variations for testing the imaging quality of three IR-783@BSA complexes. The imaging outcomes were also different with NIR-II modality due to the suppressed tissue autofluorescence and scattering. Nevertheless, three complexes indeed afforded much improved circulation time and imaging quality.

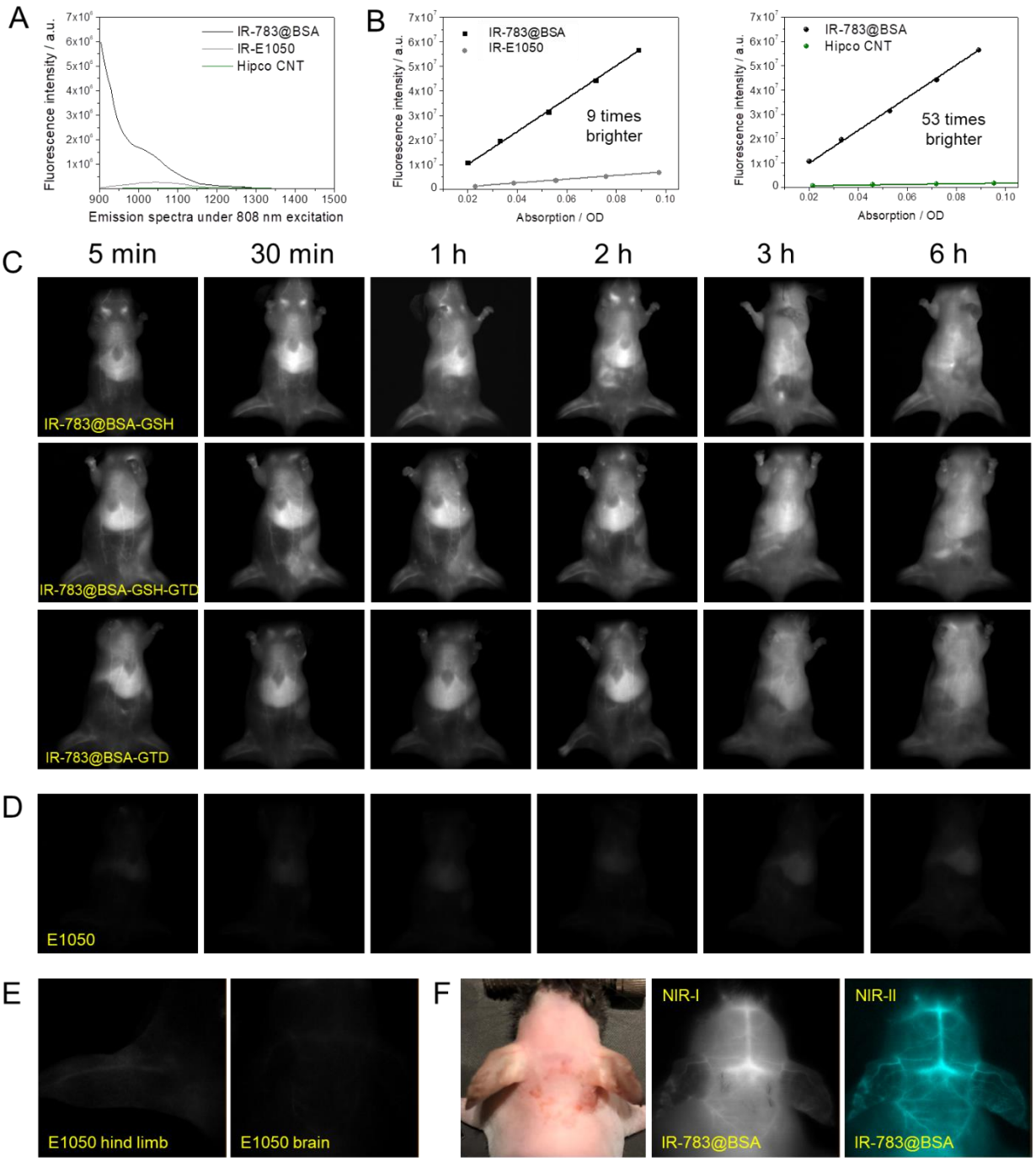


**Fig. S9. NIR-II QY of the IR-783@BSA complex and NIR-II vessel imaging in whole-body mode.** (**A**-**B**) Comparison of fluorescence intensity and QY of IR-783@BSA complex with IR-E1050 (*14*) and Hipco-SWCNT, indicating that IR-783@albumin complex yielded 9 times and 53 times higher QY than IR-E1050 and Hipco-SWCNT, respectively. The NIR-II quantum yield of IR-783@BSA complex was measured using an InGaAs camera with both IR-E1050 and Hipco CNT as references (*13*, *35*, *51*). (**C**) Typical NIR-II imaging (over 1200 nm long pass filter) of IR-783@BSA complex injected mice at belly angel. The prolonged circulation time and enhanced quantum yield of IR-783@BSA complex afford high resolution vessel imaging. (**D**) Typical NIR-II imaging (over 1200 nm long pass filter) of IR-E1050 with the same imaging condition in C. (**E**) 2.5× magnification imaging mouse hindlimb and brain with IR-E1050 failed to record the vessel structure (imaging condition is the same with Fig. 4C in main text). (**F**) Side-by-side brain imaging in both NIR-I and NIR-II window through the same imaging camera demonstrated the

advantage of the proposed technology (novel probe and NIR-II imaging window) compared with the commonly used NIR-I imaging modality.

**Note:** IR-E1050 and Hipco CNT, the typically used NIR-II dyes with peak emission in the NIR-II region, were not bound to BSA. The QY of IR-783@BSA complex is 0.4% × 53 = 21.2% (the QY of Hipco CNT is 0.4%) (*13*, *17*, *52*).

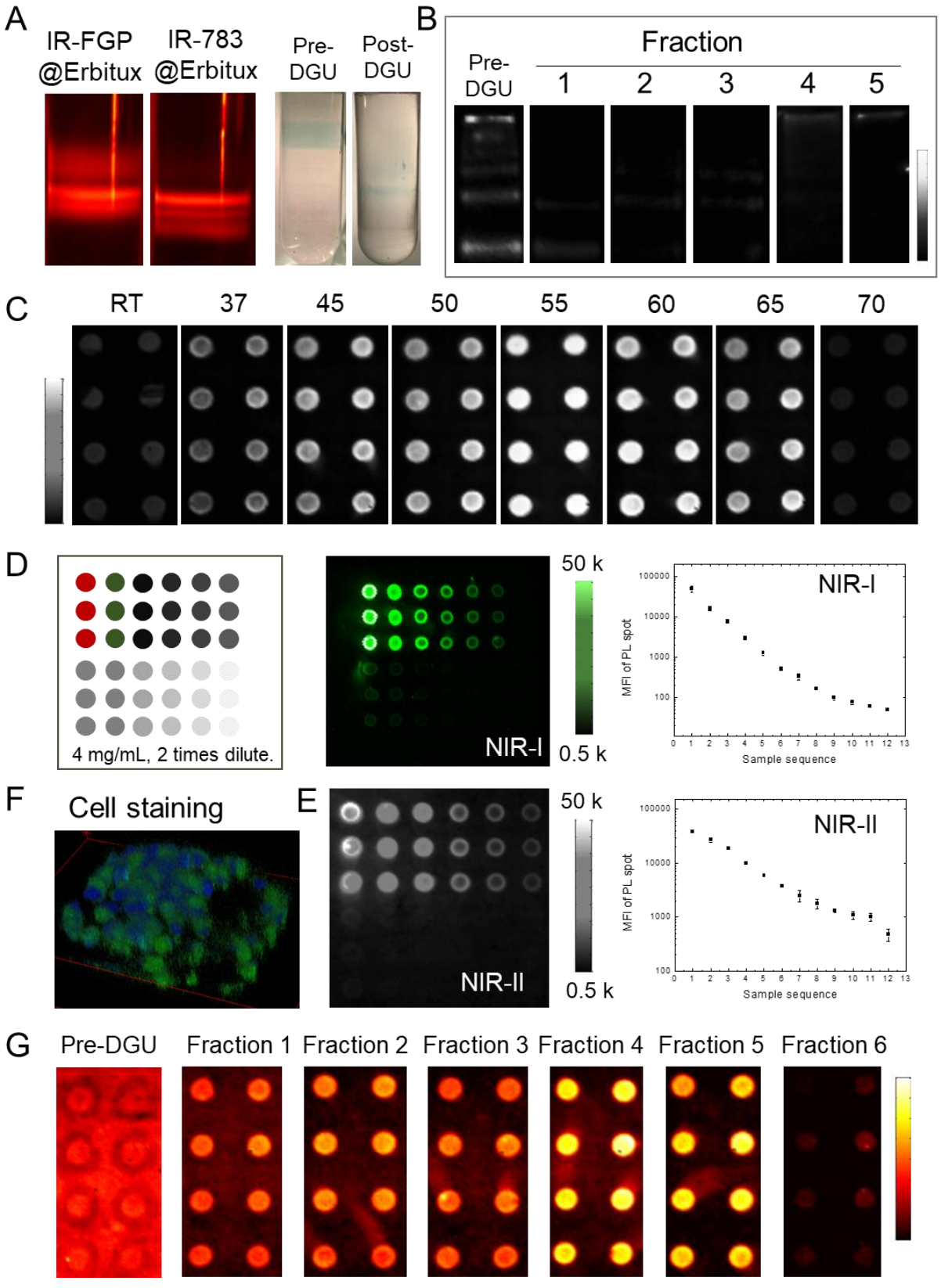
A
IR-FGP @Erbitux
IR-783 @Erbitux
Pre-DGU
Post-DGU
B
Fraction
Pre-DGU
1
2
3
4
5
C
RT
37
45
50
55
60
65
70
D
4 mg/mL, 2 times dilute.
NIR-I
50 k
0.5 k
NIR-I
MFI of PL spot
Sample sequence
F
Cell staining
E
NIR-II
50 k
0.5 k
NIR-II
MFI of PL spot
Sample sequence
G
Pre-DGU
Fraction 1
Fraction 2
Fraction 3
Fraction 4
Fraction 5
Fraction 6

**Fig. S10. The IR-783@Erbitux complex afforded an efficient conjugate and decent targeting ability for molecular imaging.** (**A**) Complex reaction detail and DGU purification of the final IR-783@Erbitux complex compared with IR-FGP@Erbitux conjugate. (**B**) Electrophoresis gel test of pre-DGU and post-DGU fraction samples. (**C**) Assay of binding affinity (on SCC cell lysate) of complex at different heating temperature (55-65 $^{O}$C is the optimal reaction temperature range). (**D**-**E**) Reverse phase protein lysate microarray (RPPA) test of the IR-783@Erbitux complex at both NIR-I and NIR-II windows on SCC cell lysate. The IR-783@Erbitux complex exhibited comparable targeting capacity compared with IRDye800cw labeled Erbitux. (**F**) SCC cell staining of IR-FGP@Erbitux conjugate. (**G**) RPPA test of the IR-FGP@Erbitux conjugate on SCC cell lysate. Comparing between IR-FGP@Erbitux conjugate and IR-783@Erbitux complex, the IR-783@Erbitux complex (60 $^{O}$C heated one) exhibited improved signal to background ratio (~6) compared with IR-FGP@Erbitux conjugate (~5) (the typical covalent NIR-II conjugate) (*37*).

**Note:**

1. Density gradient ultracentrifugation, a technique whereby a buoyant density or sedimentation coefficient difference drives biomolecule separation during ultracentrifugation after establishing a linearly changing density gradient along the length of a centrifuge tube, demonstrated excellent separation of the various species within the reaction mixture post-bioconjugation (*37*). The detailed steps were listed as follows:
   1) The sucrose column gradient for 4 mL DGU tube was made by interval adding 400 μL 10, 15, 20, 25, 30, 35, 40 % sucrose solutions in sequence. Using the syringe needle cutting into the lower layer can prevent disturbance.
   2) Once seven layers were added in sequence without obvious disturbance, the interface can be visualized by naked eyes.
   3) Put the tube tilting for 45 min at 20° angle, and the linear gradient will be formed.
   4) Add the sample (200 μL) on the top the column.
   5) Add the protecting PBS buffer on the top of the sample layer, making the tube completely full.
   6) Subject the tube to ultracentrifuge for 18 hours at 50000 rpm and 4 ℃.
   7) The DGU sample was collected by fractionating and further using.
   8) Sucrose column gradient for 50 mL DGU tube was made by gradient maker: from 20% to 50 % (16 mL). 5 mL 60 % sucrose was firstly added at the bottom of the tube before forming gradient. Then subject to ultracentrifuge for 48 hours at 31000 rpm and 4 $^{O}$C.
2. Complex formed conditions: protein with/without GSH/GTD: 13 μM; dye: 10 μM; 60 ℃ for 30 min. Purified by DGU and PL imaging.
3. Although not fully achieved in the current work, the present complex strategy can also be used in other sulfonated dyes (*13*) and even hydrophobic dye structures.